Available online at www.sciencedirect.com
SCIENCE DIRECT®
C. R. Chimie 7 (2004) 521–527
COMPTES RENDUS CHIMIE

Preliminary communication / Communication

From molecules to materials: some examples in yttrium and lanthanide chemistry

Liliane G. Hubert-Pfalzgraf *, Stéphane Daniele

IRC, université Claude-Bernard–Lyon-1, 2, av. Albert-Einstein, 69626 Villeurbanne cedex, France

Received 19 July 2003; accepted after revision 12 March 2004

Abstract

Hydrolytic and hydrothermal transformations were applied to yttrium alkoxides, namely $Y_5O(O^iPr)_{13}$, $Y_3(O^tBu)_9(^tBuOH)_2$ and $[Y_8O_6(O^tBu)_{12}]_m$. The resulting powders were characterized by XRD, TGA and transmission electron microscopy (TEM). Hydrolysis of the octanuclear oxo species gave nanocrystalline (5–6 nm) cubic Y_2O_3 at 400 °C by annealing of an oxohydroxide. Hydrothermal transformation in basic media (200 °C, 10 h, 17 atm) of $Y_5O(O^iPr)_{13}$ gave amorphous Y_2O_3 as well as crystalline platelets and nanowires of $Y(OH)_3$. Transformation into cubic yttria was achieved at 300 °C. The lability of the M–OR bond allows easy formation of mixed-metal species, giving access to doped materials of high homogeneity and crystallinity, as shown by a Y_2O_3 matrix doped by Pr_2O_3. Modification of $Y_5O(O^iPr)_{13}$ by polymerisable ligands provided molecular oxohydroxide aggregates that can be used for access to organic-inorganic materials by copolymerisation reactions. ***To cite this article: L.G. Hubert-Pfalzgraf, S. Daniele, C. R. Chimie 7 (2004).***

Résumé

Des transformations hydrolytiques et hydrothermales ont été appliquées à des alcoxydes de l'yttrium, tels que $Y_5O(O^iPr)_{13}$, $Y_3(O^tBu)_9(^tBuOH)_2$ et $[Y_8O_6(O^tBu)_{12}]_m$. Les poudres obtenues ont été caractérisées par diffraction des RX, ATG et microscopie électronique à transmission. L'hydrolyse de $[Y_8O_6(O^tBu)_{12}]_m$ conduit à Y_2O_3 cubique et nanocristallin (5–7 nm) dès 400 °C. La transformation hydrothermale en milieu basique (200 °C, 10 h, 17 atm) de $Y_5O(O^iPr)_{13}$ donne Y_2O_3 amorphe et des plaquettes et nanofils cristallisés de $Y(OH)_3$. La conversion en Y_2O_3 cubique est achevée dès 300 °C. La labilité de la liaison M–OR permet un accès facile à des alcoxydes hétérométalliques et à des oxydes dopés présentant une grande homogénéité ou cristallinité. Ceci est illustré par l'obtention d'une matrice de Y_2O_3 dopée par Pr_2O_3. La modification de $Y_5O(O^iPr)_{13}$ par des ligands polymérisables conduit à des agrégats oxohydroxyde octanucléaires et à des matériaux organiques–inorganiques par copolymérisation. ***Pour citer cet article : L.G. Hubert-Pfalzgraf, S. Daniele, C. R. Chimie 7 (2004).***

Keywords: Lanthanides; Nanomaterials; Alkoxides; Multimetallic oxides; Polymerisable ligands; Organic–inorganic materials; Sol–gel

Mots clés : Lanthanides ; Nanomatériaux ; Alcoxydes ; Oxydes multimétalliques ; Ligands polymérisables ; Matériaux organiques–inorganiques ; Sol–gel

* Corresponding author.
E-mail address: hubert@univ-lyon1.fr (L.G. Hubert-Pfalzgraf).

doi:10.1016/j.crci.2004.03.001

1. Introduction

Metal alkoxides represent one of the most common and attractive class of metal precursors for advanced oxide materials. Their interest lies in an easy access, the ability to tune their properties by modification of their coordination sphere in order to achieve the requirements for solution but also vapour phase chemical processes as well as their ability to provide homogeneity at a molecular level for multimetallic oxides via the formation of heterometallic species [1]. By contrast to most main group and transition metals, lanthanide alkoxides did not receive much attention until the last decade, although rare earth oxide materials are involved in a variety of high-tech applications [2]. Isopropoxides are representative of simple metal alkoxides that offer a high ceramic yield as well as most of the properties, especially solubility, required for applications in material science. While those are generally oligomers or solvates as illustrated by $[Al(O^iPr)_3]_4$ or $[Zr(O^iPr)_4(^iPrOH)]_2$, more complex architectures are observed for lanthanides due to their demand for high-coordination numbers and their trivalent nature. The basic structural unit is a pentanuclear core corresponding to an oxoalkoxide $Ln_5(\mu_5\text{-}O)(O^iPr)_{13}$ resulting from desolvation and linking of intermediate solvates. Those are more stable for tertiobutoxides affording isolable $Ln_3(O^tBu)_9(^tBuOH)_2$ species but desolvation remains facile providing oxoalkoxides such as $Ln_5(\mu_5\text{-}O)(O^tBu)_{13}$ (Ln = La, Nd, Yb) or of higher nuclearity, $[Y_8O_6(O^tBu)_{12}]_m$, for yttrium [3].

We wish to report herein preliminary results illustrating the potential of yttrium alkoxides for access to nanocrystalline pure and doped yttrium oxide at low temperature as well as doped organic polymers.

2. Experimental

All molecular compounds were prepared under inert atmosphere using Schlenk tubes and vacuum line techniques and characterized as previously reported [4]. Analytical data were obtained from the 'Centre de microanalyses du CNRS'. Homo- and copolymerization reactions were done under inert atmosphere in the presence of 2,2′-azobis(2-methylpropionitrile) (AIBN, 2% molar / C=C functionalities). Styrene was distilled in order to remove the stabilizer. Polymerisation was quenched by addition of alcohol.

Hydrothermal reactions (200 °C, 10 h, 17 atm) were performed with deionised water in the presence of four equivalents of $NH_3{\cdot}H_2O$. Precipitates were washed with water until the pH of the medium was neutral. After dialysis during three days, they were dried at 100 °C. The as prepared powders issued from hydrolyses were dried under vacuum at rt for 6 h. Compositions of the powders were reached by elemental analysis, FT–IR and X-ray diffraction (XRD) (Cu Kα radiation, Siemens D5000 diffractometer). Size and morphology were observed by transmission electron microscopy (TEM) with a Philips CM12 spectrometer at 100 kV. EDX data were collected on a JEOL 2010 electron microscope. TGA and DTA were conducted under air using a Setaram system (heating rate 5 °C min^{-1}). XPS data were obtained with an Escalab 200R (VG Scientific) spectrometer using the Kα Al radiation as excitation source. Fluorescence spectra were obtained using excitation with a Xe lamp and a JY H10D monochromator (λ = 430 nm). Light was collected with an UV optical fibre coupled to a JY TRIAX 320 and a CCD camera (1200 g/320 nm grating, integration time 1 s, resolution 0.65).

3. Results and discussion

3.1. The quest for low-temperatures routes to Y_2O_3

Yttrium oxide has a number of applications such as high index oxide for dielectric mirrors for high power UV lasers, transparent matrices for phosphors and doping with Eu, Tb [5] and Pr [6], catalyst support or even catalysts [2]. Improved performances are obtained with nanocrystalline oxides for most applications, the activity of nanocrystalline Ln_2O_3 for the reduction of nitrogen oxides being comparable to that of Co-ZSM-5 [7]. Most methods for access to yttria are based on thermal decomposition or precipitation reactions of their salts [8], leading to quite high (> 600 °C) temperatures of crystallization of the oxide. Herein, we have considered various wet transformations processes of metal alkoxides in order to overcome the high stability of yttrium or lanthanide hydroxides on the route to oxides and accede to nanocrystalline arrays.

3.1.1. Room-temperature hydrolytic conversions

Hydrolyses of $Y_3(O^tBu)_9(^tBuOH)_2$ (**Y3**), $Y_5(\mu_5\text{-}O)(O^iPr)_{13}$ (**Y5**) and $[Y_8O_6(O^tBu)_{12}]_m$ (**Y8**) in THF

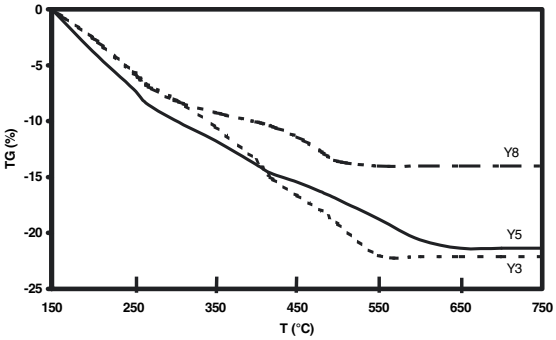

Fig. 1. TGA patterns under air of the powders derived from **Y3, Y5** and **Y8**, respectively.

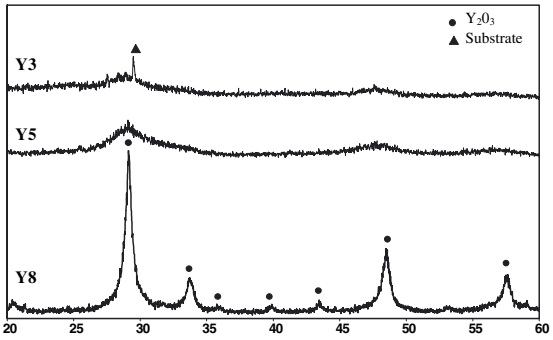

Fig. 2. XRD patterns of the powders derived from **Y3, Y5** and **Y8** calcinated at 400 °C.

(0.02–0.03M) at rt with a large excess of deionised water (hydrolysis ratio h = mole H_2O/mole precursor = 300, 500 and 800 respectively) gave amorphous powders. In contrast, crystalline hydroxides $Ln(OH)_3$ were obtained for lanthanum, praseodymium and neodymium alkoxides [9]. FT–IR spectra of the powders derived from **Y5** and **Y8** were similar, showing no organics, by comparison to those derived from **Y3**. TGA data and elemental analysis accounted for the formation of $Y(OH)_3{\cdot}H_2O$ for **Y3** and **Y5** and of $Y_2O(OH)_4{\cdot}4.3\ H_2O$ for **Y8**. TGA data showed several thermal events (Fig. 1). Anhydrous $Y(OH)_3$ and $Y_2O(OH)_4$ were obtained at 150 °C. Weight losses for powders derived from **Y3** and **Y5** occurred in three steps (≈ 7%) over the range 150–600 °C. The TGA pattern of **Y8** showed two well-defined weight losses (9.2 and 4.5%) between 150 and 300 °C and up to 500 °C. All losses were endothermic corresponding to elimination of OH ligands and could be summarised by Eqs. (1) and (2) for the powders of **Y3, Y5** and **Y8**, respectively:

$$\mathbf{Y3,Y5:}\ Y(OH)_3 \xrightarrow{150^\circ C\ 275^\circ C} Y_2O(OH)_4 \xrightarrow{275^\circ C\ 420^\circ C} YO(OH) \xrightarrow{420^\circ C\ 600^\circ C} Y_2O_3 \quad (1)$$

$$\mathbf{Y8:}\ Y_2O(OH)_4 \xrightarrow{150^\circ C\ 300^\circ C} Y_2O_{2.5}(OH) \xrightarrow{300^\circ C\ 500^\circ C} Y_2O_3 \quad (2)$$

Powders derived from **Y8** showed the lowest weight loss, this being associated with the lowest temperature of complete removal of –OH groups. Hence annealing powders derived from **Y8** at 400 °C for 4 h gave well-crystallized cubic yttria, while crystallization was only starting for the powders derived from **Y3** and **Y5** (Fig. 2) – the temperature of crystallization by annealing (4 h) was lower than that observed by TGA, which is a dynamic process. TEM of powders derived from **Y8** showed that Y_2O_3 was composed of spherical nanocrystallites of about 5–6 nm aggregated into submicron secondary particles (Fig. 3A). HRTEM images illustrate the high crystallinity of Y_2O_3 even at 400 °C, since no amorphous layer was observed on the surface of the nanoparticles and all diffraction peaks could be attributed (Fig. 3A and C). These data illustrate that the increase of the number O^{2-} ligands in the precursor favours the obtaining of a crystalline oxide array at low temperature. By comparison, a sol of $Y(OH)_{3-x}(NO_3)_x$ ($x \approx 0.5$) obtained from $Y(NO_3)_3$ by anion exchange in

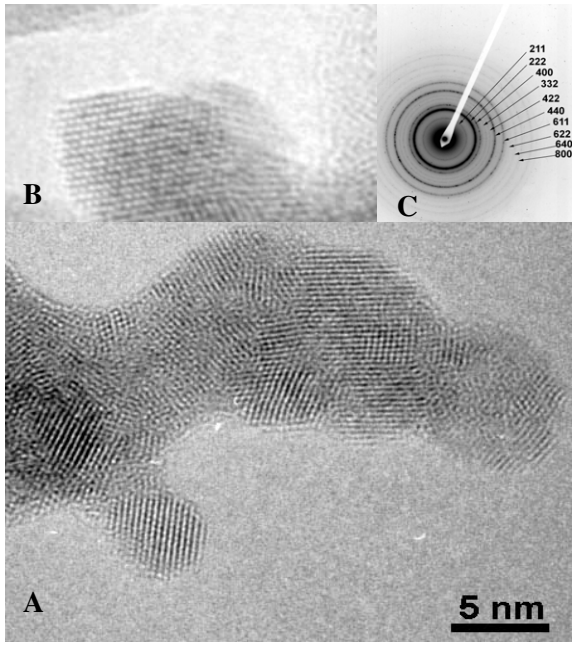

Fig. 3. (**A**) TEM image, (**B**) HR–TEM image, and (**C**) diffraction peaks of the powder derived from **Y8** calcinated at 400 °C.

basic aqueous media required annealing above 600 °C for crystallisation of cubic Y_2O_3 [10].

3.1.2. Hydrothermal transformations

Hydrothermal transformations have been largely used in material science for access to nanoparticles and/or special microstructures [11].

The hydrothermal transformation in the presence of ammonia of $ScCl_3{\cdot}6\ H_2O$ affording ScO(OH) [12] prompted us to use a similar approach (200 °C, 10 h, 17 atm) for yttrium [13]. However, conversion of $YCl_3{\cdot}6\ H_2O$ gave a crystalline chlorohydroxide (JCPDS 30-1445) $Y_2(OH)_{4{\cdot}86}Cl_{1.14}(H_2O)_{0.7}$ due to the poor lability of the Y–Cl bonds. The use of alkoxides, $Y_5O(O^iPr)_{13}$ or $Y_3(O^tBu)_9(^tBuOH)_2$ (0.05 M) as reagents in similar conditions afforded amorphous oxide in both cases. The presence of oxide in those powders was evidenced in the FT–IR by its characteristic Y–O absorption bands (560, 460 cm^{-1}), whereas absorptions at 3615 and at 3408 cm^{-1} accounted for hydroxide species. XRD patterns for the powders derived from **Y5** indicated cubic Y_2O_3 mixed with the hexagonal hydroxide $Y(OH)_3$ phase. TEM confirmed the crystallinity of the powders and moreover showed their polymorph nature (Fig. 4). Three types of morphology were observed although needles and nanorods (700 × 10 up to 6000 × 200 nm) were predominant. Lanthanide hydroxide nanowires obtained by hydrothermal treatment of colloidal suspensions of $Ln(OH)_3$ were reported recently but no data were given for yttrium [14]. TGA analysis allowed further identification of the various phases. The total mass loss was 12.4% for the powder issued from **Y5**, suggesting a composition of 65% $Y(OH)_3$ and 35% Y_2O_3. Transformation into cubic yttria was complete at 300 °C, the lowest temperature reported so far for this oxide.

TEM micrographs of the powders resulting from **Y3** indicated mostly amorphous nearly spherical particles of about 35 nm diameter, crystalline platelets (200 × 200 nm to 400 × 400 nm) and crystalline needles (10-nm diameter, 450–700-nm length). The weight loss (8.2%) indicated a higher proportion of oxide than for those derived from **Y5**. Indeed, conversion of *t*-butoxides into oxides is generally favoured over that of isopropoxides due to formation of isobutylene as observed in MOCVD [1]. The TGA data suggest either a composition of 61.6% Y_2O_3 and 38.4% $Y(OH)_3$ or nearly only YO(OH) (a weight loss of 7.4%

Fig. 4. TEM image of powder derived from hydrothermal treatment of **Y5**.

is expected). The latter assumption is not very likely due to the presence of Y_2O_3 in the FT–IR and oxolation has been reported to be difficult for yttrium [15]. Surprisingly, in contrast with the powder issued from **Y5**, conversion into crystalline yttria under air required more than 900 °C. The difference between the powders derived from **Y3** and **Y5** might be related to their surface properties. Indeed, close examination of the FT–IR suggests the presence of carbonate ligands for the powders derived from **Y3** (absorptions at 1790, 1525, 1405 cm^{-1}) [16]. Carbonation might thus control here the temperature of crystallization, but the reactivity of those powders was not further investigated.

3.2. Toward highly homogeneous multimetallic materials

The stereolability of metal alkoxides or oxoalkoxides allows the formation of mixed-metal species by mixing of homometallic species at rt providing homogeneity at a molecular level for multimetallic materials [1,2]. The reaction between $Y_5(\mu_5\text{-}O)(O^iPr)_{13}$ and $Pr_5(\mu_5\text{-}O)(O^iPr)_{13}$ (4:1 stoichiometry) in THF gave $Y_4Pr(\mu_5\text{-}O)(O^iPr)_{13}$ having a structure similar to that of

the Ln_5O_{14} core as established by single crystal X-ray studies [17]. Its hydrolysis (THF, 0.025 M, h = 500) afforded an amorphous pale green powder whose elemental analysis indicated a ratio Y:Pr of 4, as in the precursor. TGA analysis in air exhibits three weight losses of 9.7, 7.7 and 9.3% within the temperature ranges of 50–150, 150–300 and 300–700 °C. These overall data account for the formation of hydrated $Y_4PrO_{0.5}(OH)_{14}$ with the loss of adsorbed water being followed by the elimination of the –OH groups (Eq. (3)):

$$Y_4PrO_{0.5}(OH)_{14} \xrightarrow{150^\circ C\ 300^\circ C} Y_4PrO_4(OH)_7 \xrightarrow{300^\circ C\ 700^\circ C} 4Y_2O_3{:}Pr_2O_3 \quad (3)$$

XRD studies indicated that the onset of crystallisation of cubic Y_2O_3 was higher by about 100 °C (from 400 to 500 °C) compared to $Y_5(\mu_5\text{-}O)(O^iPr)_{13}$ (cf. § 3.1.1). At 500 °C, the colour of the solid changes from pale green to deep orange. Cubic Y_2O_3 was the only crystalline phase observed up to 900 °C. The slight decay of the 2θ peak values compared to pure Y_2O_3 suggests that Pr atoms were incorporated in the network of the Y_2O_3 matrix. Average particle sizes were estimated to range from 7.7 to 15.3 nm between 500 and 900 °C according to the Scherrer equation. TEM and X-ray Energy Dispersive (EDX) data indicated a very homogeneous Pr distribution (6.75 atomic%) in the Y_2O_3 array. X-ray photoelectron spectroscopy (XPS) (0–1000 eV) displayed peaks due to O^{2-}, Y^{3+} and Pr^{3+} atoms. No peak due to Pr^{4+}atoms was observed. The O1s spectra displayed two broad peaks at 531.5 and 528.7 eV different from the O^{2-} contributions of Y^{3+}–O and Pr^{3+}–O bonds in Y_2O_3 and Pr_2O_3 (530.5 and 529.3 respectively) [18]. This confirms that, despite the differences of the Y_2O_3 and Pr_2O_3 structures, Pr^{3+} atoms could substituted Y^{3+} ones in the Y_2O_3 lattice to form luminescent centres. Hence photoluminescence spectra (PL) were observed at rt for the samples calcinated at 500 °C in the IR (800–850 nm) (Fig. 5). They can be ascribed to the spin-allowed ($^1D_2 \rightarrow {}^3H_6$, $^3F_2$) transition of Pr^{3+} centres via their (4f)(5d) excited state. Peaks were very sharp accounting for the high crystallinity of the sample. Very homogeneous nanosized lanthanide-doped Y_2O_3 materials can thus be obtained at low temperature starting from multimetallic precursors by comparison to coprecipitation reactions.

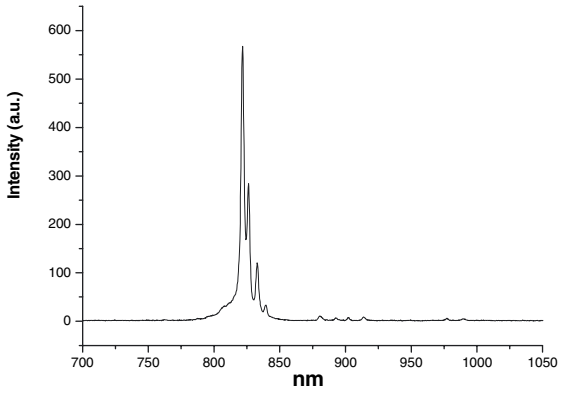

Fig. 5. Photoluminescence spectra of the powder derived from $Y_4Pr(\mu_5\text{-}O)(O^iPr)_{13}$ calcinated at 500 °C.

3.3. Alkoxides with polymerisable ligands: toward hybrid materials

The preceding examples have illustrated access to extended inorganic arrays by formation of M–O–M bonds. Yttrium and lanthanide alkoxides are active living ring-opening catalysts of lactones or lactides for instance affording biomaterials and thus organic networks [19]. Organic-inorganic materials such as doped polymers are other attractive materials [20]. Homo- or copolymerisation reactions based on $M(OR)_{n-x}Z_x$ species, where Z is a polymerisable ligand, allow access to extended organic arrays as well as inorganic ones [21]. Better homogeneity is reached when covalent association between organic and inorganic networks is achieved, the M–Z linkage thus should be stable thermodynamically and kinetically. This is achieved via Si–C bonds for silicon, but via oxygen ligation for most other elements. Chelating or bridging-chelating ligation is preferable, allylacetatoacetate (HAAA) and 2-(methacryloyloxy)ethyl acetoacetate (HAAEMA) are possible ligands.

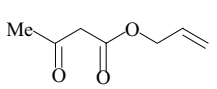

HAAA

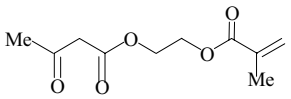

HAAEMA

The lability of the M–OR bond makes metal alkoxides choice precursor for molecular design of oxide precursors [1]. The reaction between $Y_5O(O^iPr)_{13}$ and AAAH in toluene (1:5 stoichiometry) at rt gave com-

pound **1** in quantitative yield. Its FT–IR and proton NMR data (two types of magnetically non-equivalent AAA ligands in a 2:3 ratio) account for a formula $Y_4O(O^iPr)_5(AAA)_5$. **1** is extremely unstable toward moisture; repeated attempts to get single crystals gave another, more stable compound resulting from hydrolysis–polycondensation. The crystals resulting from crystallization in ethanol/ligroine, **1a**, displayed a sharp absorption at 3357 cm^{-1} in its FT-IR spectrum, suggesting the presence of hydroxide ligands. Its ^1H NMR data indicated a decrease in the integration ratio, down to 6:10, between alkoxide namely ethoxide and AAA ligands, the latter displaying still two sets of resonances in a 2:3 ratio. The identity of **1a** was established by single crystal X-Ray diffraction (monoclinic, space group *C*2/*c*, a = 21.556(4), b = 18.752(4), c = 29.485(6) Å, β = 100.11(3)] It corresponds to an octanuclear species based on the assembly of two $[Y_4(\mu_4\text{-}O)(AAA)_5(\mu\text{-}OEt)_2]$ flattened tetrahedron via triply-bridging hydroxide O(101) and O(102) and ethoxide O(70) ligands giving a centrosymmetric $[Y_4(\mu_4\text{-}O)(\mu,\eta^2\text{-}AAA)_2(\eta^2\text{-}AAA)_3(\mu\text{-}OEt)_2]_2(\mu_3\text{-}OH)_4(\mu_3\text{-}OEt)_2]$ species (Fig. 6). Six of the metals are seven-coordinate, bearing terminal-chelating allylacetatoacetate ligands, whereas Y(4) and Y(4)# are octacoordinated, with two bridging-chelating AAA ligands. The Y_8O_{32} core is quite compact [Y(3)....Y#(3) 8.776 Å] and can be seen as a small piece of yttrium oxohydroxide wrapped with polymerisable ligands. The formation of **1a** results from the hydrolytic condensation of two $Y_4O(OR)_5(AAA)_5$ formally derived from substitution of five OR groups of $Y_5O(OPr^i)_{13}$ and elimination of a basal $Y(OR)_3$ moiety (Eqs. (4) and (5)).

$$Y_5O(OiPr)_{13} + 5HAAA \rightarrow Y_4O(OiPr)_5(AAA)_5 + 1/m[Y(OiPr)_3(PrOH)_x]_m + 5 - x/m\ HOiPr \quad (4)$$

$$2\ Y_4O(OiPr)_5(AAA)_5 \xrightarrow{EtOH,\ H_2O} Y_8O_2(OH)_4(OEt)_6(AAA)_{10} + 5\ HOiPr \quad (5)$$

Similar results were obtained with $Y_5O(O^iPr)_{13}$ and 2-(methacryloyloxy)ethyl acetoacetate, although no single crystals could be grown. The reaction lead to an unstable intermediate **2** giving compound **2a** showing characteristic sharp Y–OH absorptions in the IR (3658 cm^{-1}) as well as the absorption bands of the $\nu_{C=O}$ and $\nu_{C=C}$ vibrations (1722, 1633, 1537, 1514 and 1505 cm^{-1}). The stability of the Y or Ln–OH bond, a hurdle for low temperature routes to oxides, allows

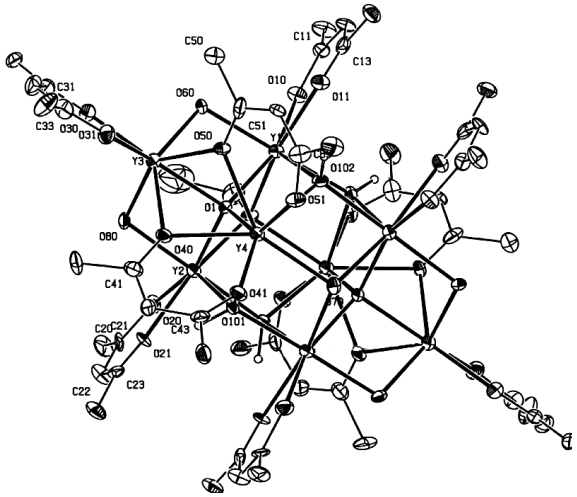

Fig. 6. Molecular structure of $[Y_4(\mu_4\text{-}O)(\mu,\eta^2\text{-}AAA)_2(\eta^2\text{-}AAA)_3(\mu\text{-}OEt)_2]_2(\mu_3\text{-}OH)_4(\mu_3\text{-}OEt)_2]$ (thermal ellipsoids at 20% probability, the chains of the AAA ligands have been removed for the sake of clarity, only the H corresponding to the OH ligands are shown). Yttrium–oxygen bond distances: 2.196(9)–2.489(10) Å with the ranking Y–μ_4-O ≤ Y–μ-OEt < Y–μ_3-OH < Y–η^2-AAA < Y–μ_3-OEt < Y–μ,η^2-AAA: Y–O(1) 2.196(9)–2.287(9), Y–μ-OEt 2.230(9)–2.276(9); Y–μ_3-OH 2.314(9)–2.398(10); Y–η^2-AAA 2.288(11)–2.403(10); Y–μ_3-OEt(O70) 2.400(9)–2.419(9); Y···Y distances 3.746(3) for Y(1)···Y(2) to 3.506(2) Å for Y(3)···Y(4). CCDC reference number: 175 661.

aggregation as molecular oxohydroxides and thus formation of clusters of unprecedented frameworks [4]. It is also noteworthy that the $Ln_5O(O^iPr)_{13}$ core behaves as a source of $Ln_4O(O^iPr)_{10}$ moieties either for heterometallics with $M(O^iPr)_4$ (M = Ti, Zr) or $Ln(O^iPr)_3$ fragments as previously shown [2] or in substitution reactions.

Homo and copolymerisation reactions were investigated for **1a** and **2a**. Thermal activation appeared better than photochemical one due to less degradation of the complexes (< 5%). As expected, formation of the organic network was favoured for **2a** with the AAEMA ligand bearing an acrylate functionality as compared to **1a**, which showed a low conversion into C–C bond formation. Homopolymerisation of **2a** was achieved in toluene at 75 °C in the presence of AIBN as initiator. After 6 h, the solution was transformed into a glassy gel indicating cross-linking. The Y–OR absorption bands at 571, 535, 480 cm^{-1} were unchanged with respect to those of **2a** indicating that gelation was not due to hydrolysis. Copolymerization of **2a** with styrene $C_6H_5CH{=}CH_2$ (stoichiometry **2a**: styrene = 20) gave a

gel after 4 h at 75 °C. Formation of the polystyrene (PS) network was evidenced by its characteristic sharp absorption bands. Longer reaction times lead to growth of the organic network with hardening and shrinkage of the gel as a glassy, transparent insoluble polymer, whereas the Y–OR absorptions bands remained unaffected. No metallic species was found in the mother liquor nor extracted by washing the polymer with isopropanol, indicating that AAEMA allowed efficient anchoring to the PS backbone. Elemental analysis of the polymeric material obtained after washing with toluene in order to remove PS confirmed the presence of yttrium (2.8% in weight). Hydrolysis of the Y-polystyrene copolymer lead to change in the FT–IR with formation of the Y–O–Y network (broad absorption bands from 880 to 450 cm^{-1}) and hydroxide at 3615 cm^{-1}. This doped PS was slightly more stable thermally than the non-doped one as shown by TGA. Its EDX mapping indicated an homogeneous distribution of the metal, whereas the Y-doped PS obtained with yttrium derivatives without polymerisable ligands displayed a concentration gradient **2a** [22] was less efficient for copolymerisation with styrene than $Ti(O^iPr)_2(AAEMA)_2$, where all acrylate functions are born by chelating ligands and are thus more accessible [20].

4. Conclusions

Metal alkoxides as illustrated here by lanthanide ones are versatile oxide precursors, their most attractive features being an easy formation of mixed-metal species for either homogeneously doped binary or homogeneous multimetallic oxides. The stability of the Ln–OH bond, a hurdle for low-temperature routes to oxides, gives access to unique molecular oxohydroxide aggregates.

References

[1] L.G. Hubert-Pfalzgraf, Inorg. Chem. Commun. 6 (2003) 102.
[2] L.G. Hubert-Pfalzgraf, New J. Chem. 19 (1995) 727 and references therein.
[3] S. Daniele, L.G. Hubert-Pfalzgraf, P.B. Hitchcock, M.F. Lappert, Inorg. Chem. Commun. (2000) 218.
[4] L.G. Hubert-Pfalzgraf, N. Pajot, R. Papiernik, J. Vaissermann, J. Chem. Soc. Dalton Trans. (1999) 4127.
[5] E.T. Goldburt, B. Kulkarni, R.N. Bhargava, J. Taylor, M. Libera, J. Lumin. 72 (1997) 190.
[6] Y. Okumura, M. Tamaya, K. Arubesaaru, N. Matsuda, H. Koike, Jpn Kokai Tokkyo Koho, 1996 7 p.; Patent No. 08081678.
[7] M.D. Fokema, J.Y. Ying, Appl. Catal. B 18 (1998) 71.
[8] N. Dasgupta, R. Krishnamoorthy, K.T. Jacob, Int. J. Inorg. Mater. 3 (2001) 143.
[9] S. Daniele, L.G. Hubert-Pfalzgraf, unpublished results.
[10] M.D. Fokema, E. Chiu, J.Y. Ying, Langmuir 16 (2000) 3154.
[11] A. Chemseddine, T. Moritz, Eur. J. Inorg. Chem. (1999) 235.
[12] V. Ripert, L.G. Hubert-Pfalzgraf, R. Papiernik, P. Belleville, Chem. Mater. 11 (2001) 1880.
[13] V. Ripert, PhD thesis, University of Nice–Sophia-Antipolis, 1998.
[14] X. Wang, Y. Li, Angew. Chem. Int. Ed. Engl 41 (2002) 4790.
[15] J. Livage, M. Henry, C. Sanchez, Prog. Solid-State Chem. 18 (1988) 259.
[16] L.M. Seaverson, S.Q. Luo, P.L. Chien, J.F. McClelland, J. Am. Ceram. Soc. 69 (1986) 423.
[17] L.G. Hubert-Pfalzgraf, S. Daniele, A. Bennaceur, J.-C. Daran, J. Vaissermann, Polyhedron 16 (1997) 1223.
[18] J.F. Moulder, W.F. Stickle, P.E. Sobol, K.D. Bomben, Handbook of X-ray Photoelectron Spectroscopy, Perkin Elmer Corporation, 1992.
[19] N. Spassky, V. Simic, M.S. Montaudo, L.G. Hubert-Pfalzgraf, Macromol. Chem. Phys. 201 (2000) 2432.
[20] L.G. Hubert-Pfalzgraf, N. Pajot, R. Papiernik, J. Vaissermann, R. Collier, J. Mater. Chem. (1999) 3027.
[21] G. Kickelbick, U. Schubert, Monat. Chem. 132 (2001) 13.
[22] (a) L.G. Hubert-Pfalzgraf, L.C. Cauro-Gamet, S. Lecocq, to be published; (b) L.C. Cauro-Gamet, PhD thesis, University of Lyons, France, 2001.